Supporting Information

A "grafting technique" to tailor the interfacial behavior of hard carbon anode for stable sodium-ion batteries

Yu Sun,‡[a] Daxian Zuo,‡[a] Chengrong Xu,[a] Bo Peng,[a] Jing-Chang Li,[a] Jie Yang,[a] Sheng Xu,[a] Xinyi Sun,[a] Haoshen Zhou[a], and Shaohua Guo*[ab]

[a]*College of Engineering and Applied Sciences, Jiangsu Key Laboratory of Artificial Functional Materials, National Laboratory of Solid-State Microstructures, Collaborative Innovation Centre of Advanced Microstructures, Nanjing University, Nanjing 210093, China. E-mail: shguo@nju.edu.cn.*

[b]*Lab of Power and Energy Storage Batteries, Shenzhen Research Institute of Nanjing University, Shenzhen 518000, China*.

‡ *These authors contributed equally to this work.*

Experimental section

The FB molecule was provided by Shanghai Aladdin Biochemical Technology Co.,Ltd. Commercial HC purchased from BTR New Material Group Co.,Ltd. The different mass ratios of FB molecules and HC (5%, 10%, and 15%) were mixed with minor condensate in acetonitrile solvent and stirred continuously for 8 h. The obtained solution was placed for 10 h at room temperature, followed by 2 h at 385.15 K to completely evaporate the solvent. Subsequently, the product was cleaned using ethanol solvent to remove residual impurities. The FHC powder was dried in 353.15 K for 10 h and then transferred to a 403.1 K vacuum environment for 24 h, during which it was lightly ground several times.

Characterization

A Bruker D8 Advance XRD device with Cu Kα radiation (λ=1.5418 Å) was used to detect crystal information of FHC and HC. A PerkinElmer, Spectrum Two-LiTa FTIR spectrometer with a detection range of 450 to 4000 cm^{-1} was employed to analyse FB molecules, HC, and FHC surface functional group information. The chemical structure and composition of the samples were recorded by a Renishaw inVia confocal Raman microscope using an air-cooled HeNe laser at 632.8 nm as the excitation light. A Thermo Scientific ESCALAB 250Xi model XPS device produced from the USA was employed to provide compositional information within the SEI layer at different etching depths. The SEI on the HC and FHC surfaces can be generated by several electrochemical cycles. After cycled, the electrodes were cleaned with a Dimethoxyethane (DME) solution to remove the electrolyte residue on the surface. We applied a AFM with Bruker Dimension ICON model to explore the morphological features and flatness of the SEIs on the HC and FHC surfaces. The morphology and surface element distribution of HC and FHC before and after cycling were

visualized by a SU8000, HITACHI SEM from Japan. A Tecnai F20, Thermo Fisher Scientific, TEM configured with Energy-dispersive X-ray spectroscopy (EDS) was utilized to obtain information such as the internal carbon layer structure of the HC and FHC and the thickness of the formed SEI. The internal compositional profile of the SEI was visualised by a TOF-SIMS 5 iontof with Cs source.

Electrochemical measurements

The optimized FHC powder, Super P, and polyvinylidene difluoride (PVDF) binder with a a mass ratio of 9:0.5:0.5 were dissolved in a suitable volume of N-Methylpyrrolidone (NMP) and stirred vigorously at 500 rpm for 5h. The above obtained slurry was uniformly coated on the cleaned copper (Cu) foil, where the height of the scraper was employed to enable the active mass (FHC) loading to be controlled at ~1.8 mg cm^{-2}. The Cu foil with active material was transferred to a vacuum oven at 393.15 K for 12 h to remove residual NMP solvent. Then, the Cu foil was cut into 12 mm diameter discs to be used as FHC anode electrodes. The preparation of HC anode and NVP cathode is similar to that of FHC. Differently, the active mass of NVP was tuned to ensure a negative/positive (N/P) ratio of ~1.2.

The SIB half-cells were assembled in an Ar-filled glove box with a H_2O and O_2 value of <0.1 ppm by using HC or FHC electrodes and Na metal counter electrodes. 70 μL of 1 M $NaPF_6$ in diglyme electrolyte was employed to act as a media to transport ions. To avoid short-circuiting the battery, Whatman glass fibre (GF/B) was selected as the separator. Similarly, SIB full-cells was coupled by using HC or FHC anode, NVP cathode, and 1M $NaPF_6$ in diglyme electrolyte, respectively. The electrochemical behaviour of the SIBs, including GCD curves, durability, stability, and rate properties, was examined on a neware battery test system. To maximize sodium storage capacity, the voltage range of HC|Na and FHC|Na half-cell can be set to 0.01–2.0 V, while that of

the NVP|Na full-cell is 1.5–3.9 V. We employed a VSP300 electrochemical workstation to perform the CV curves of the half-cell at different sweep rates (0.1–2.0 mV s^{-1}). The internal impedance information of the cell is detected *via* the electrochemical impedance spectroscopy (EIS) technique that applies an amplitude of 5mV in the frequency range of 100kHz to 100MHz.

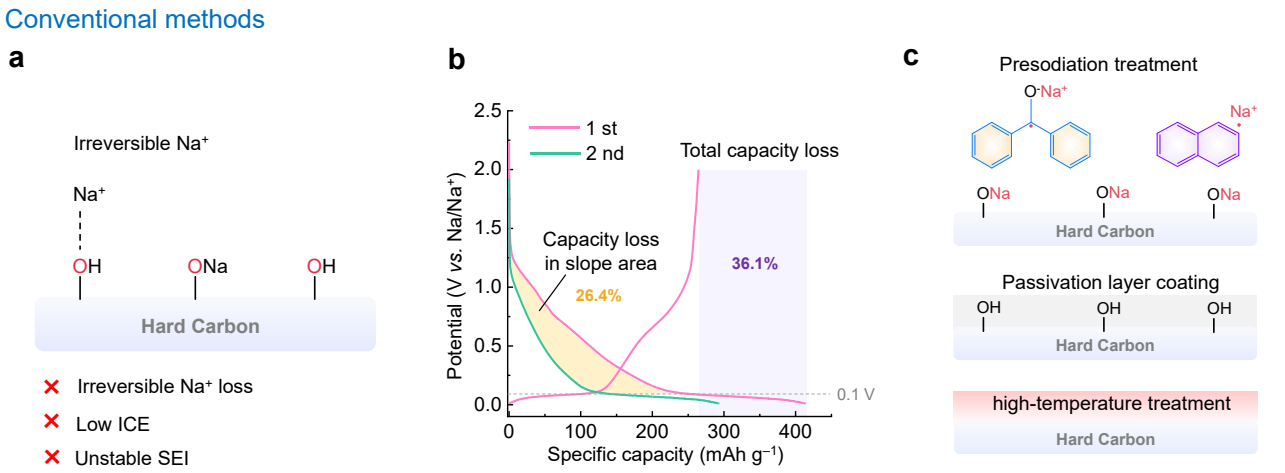

Fig. S1 (a) Commercialized HC with unfavorable functional groups caused irreversible sodium ion loss, low ICE, and unstable SEI. (b) The GCD curves of HC tested at 0.02 A g^{-1}. The sodium storage capacity in the slope area is reduced by comparing the first and second discharge curves. (c) The common treatments, including presodiation, passivation layer coating, high-temperature treatment, employed to diminish irreversible sodium loss on the surface of HC.

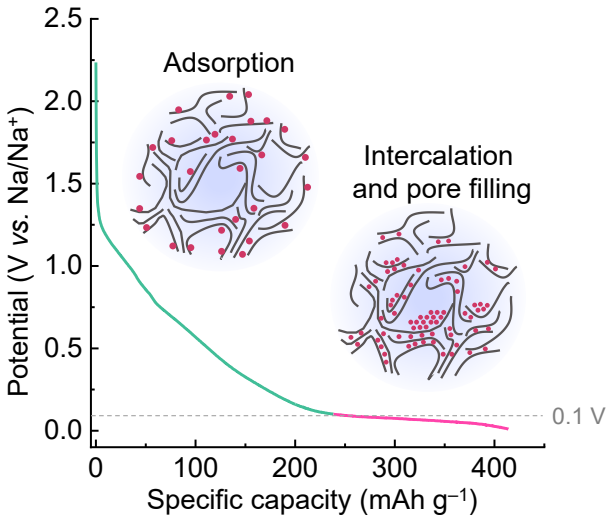

Fig. S2 The "Adsorption-Intercalation-Pore filling" sodium storage mechanism of hard carbon. The slope region (>0.1 V) capacity is mainly contributed by the hard carbon surface functional groups and defects, while the plateau region (0.1 V–0.01 V) capacity is dominated by the insertion of sodium ions between the carbon layers and the quasi-metallic sodium deposition within the closed pores.[1–3]

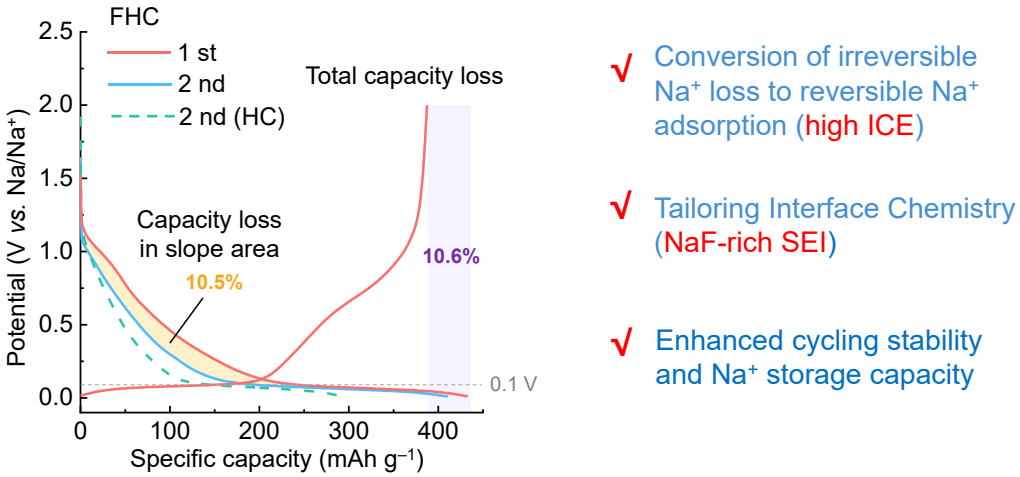

Fig. S3 The GCD curves of FHC tested at 0.02 A g^{-1}.

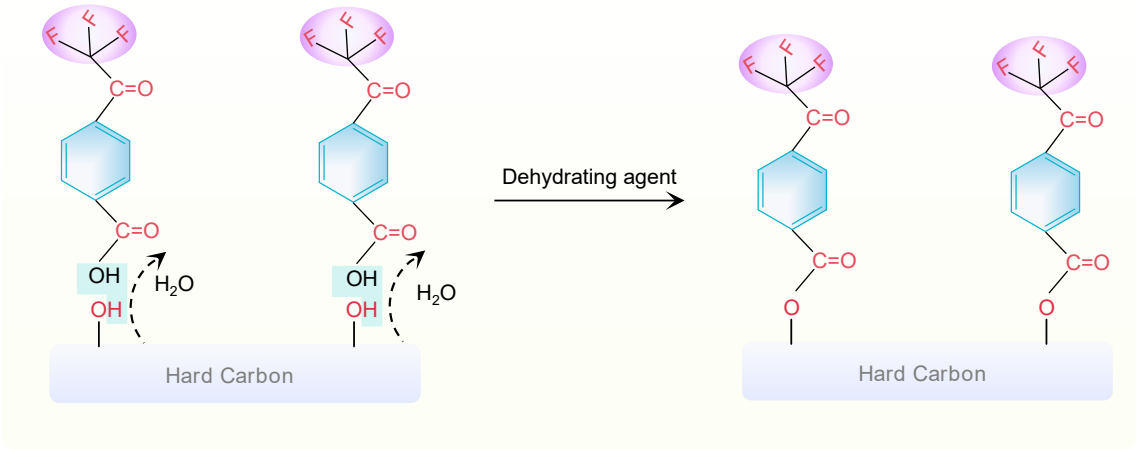

Fig. S4 FB molecules were anchored to the HC surface through a dehydration process.[4,5]

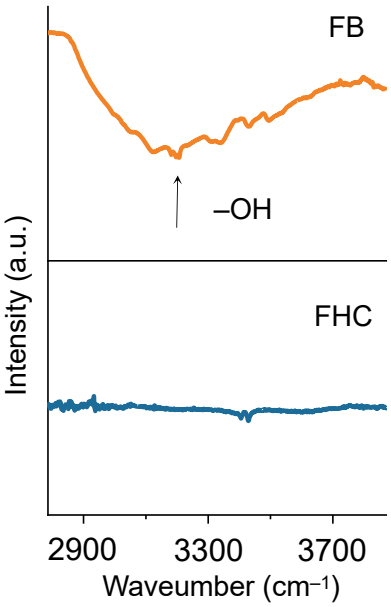

Fig. S5 The FTIR curves of FB and FHC. A broad diffraction peak located at ~3300 cm^{-1} (–OH) was observed in FB molecules, but it disappeared in the FHC, indicating that the dehydration process was finished.

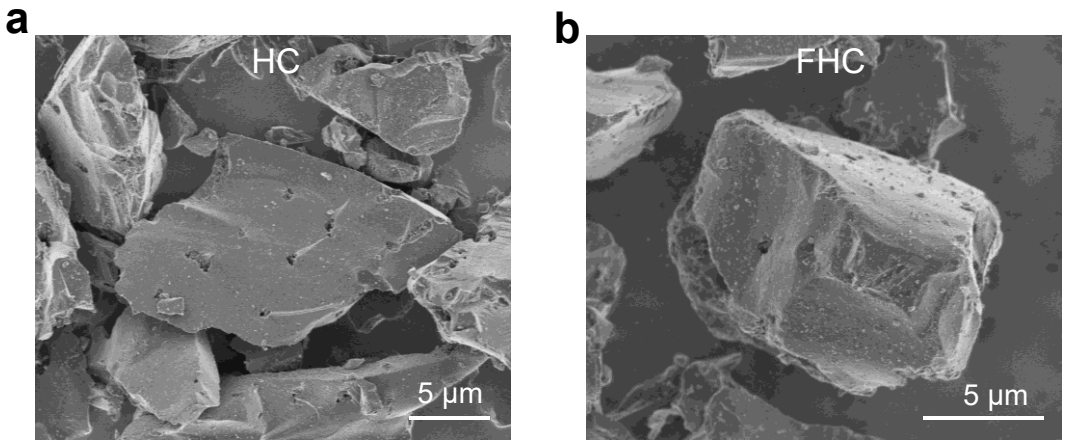

Fig. S6 SEM images of HC and FHC. Commercial HC exhibits an irregular micron-sized bulk morphology. The optimized FHC maintains the bulk profile of the HC well.

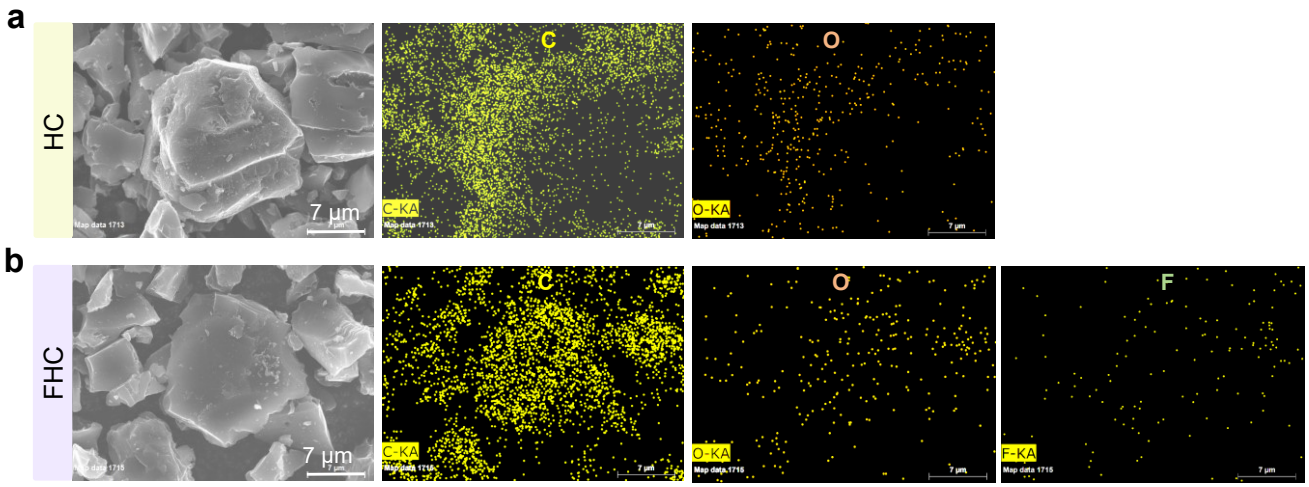

Fig. S7 Element mapping on the surfaces of (a) HC and (b) FHC.

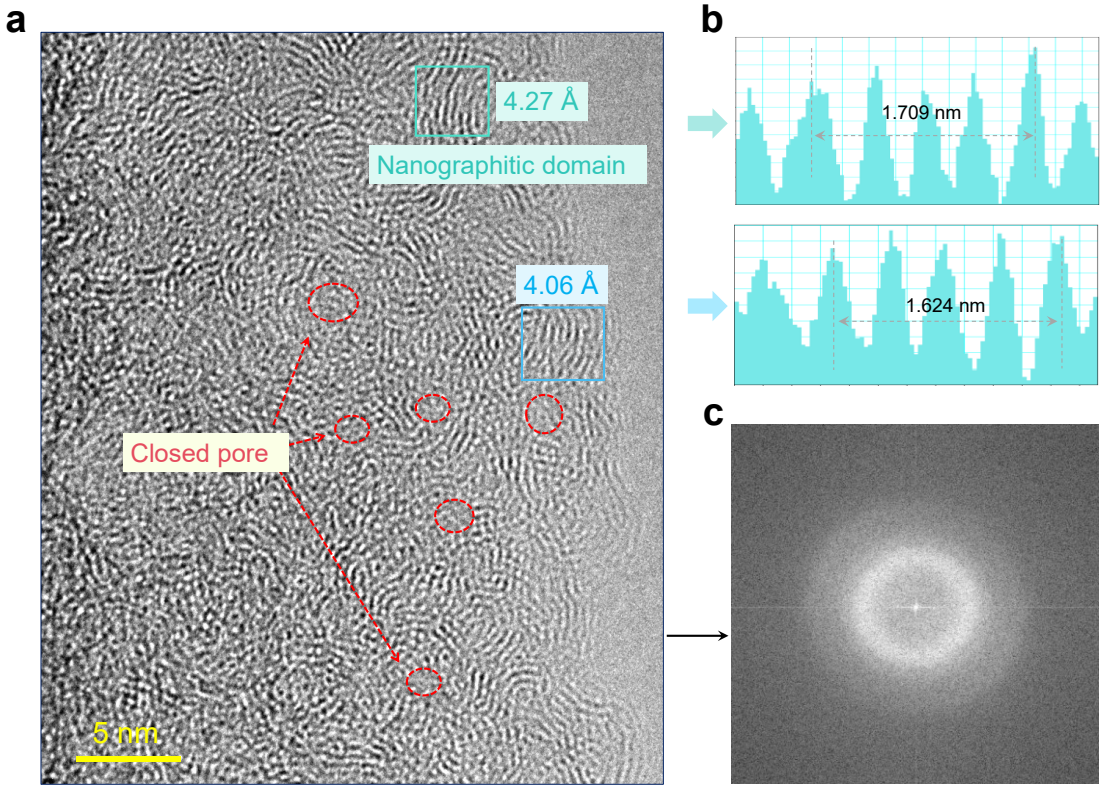

Fig. S8 (a) High-resolution TEM images of FHC. The internal structure of the FHC consists of abundant carbon layers and closed pores. (b) The carbon layer spacing is ~4.0 Å. (c) The electron diffraction ring in the region of Fig. S8a.

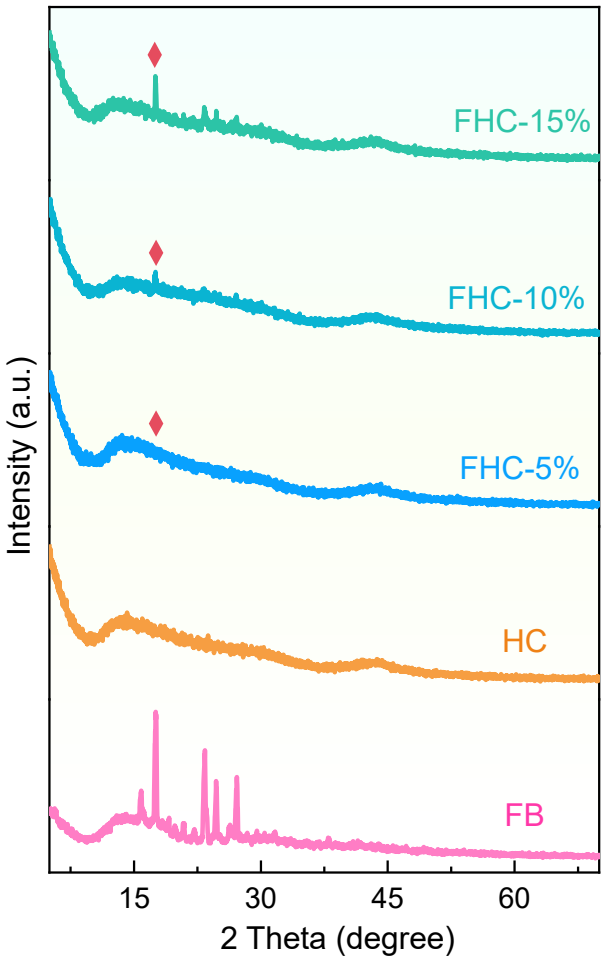

Fig. S9 XRD patterns of FB, HC, FHC-5%, FHC-10%, and FHC-15%, respectively. As the content of FB molecules increased, the HC surface presented obvious characteristic peaks of FB molecules.

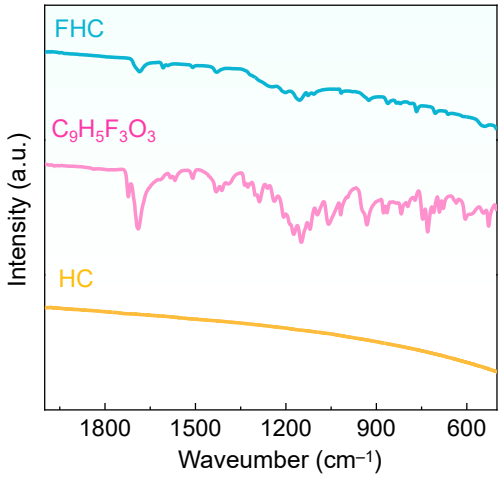

Fig. S10 The FTIR curves of FB, HC, and FHC. Compared to pure HC, the optimized FHC surface showed the functional group characteristics of FB molecules, indicating the presence of FB molecules on the HC surface.

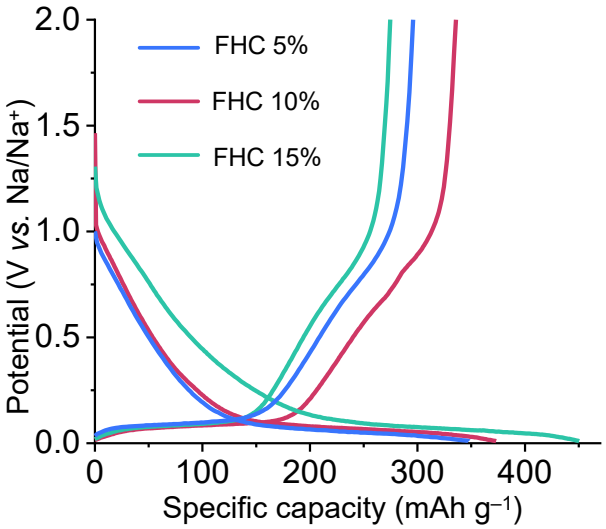

Fig. S11 The initial GCD profiles of FHC-5%, FHC-10%, and FHC-15% cycled at 0.05 A g^{-1}. Owing to the increased content of FB molecules, FHC-15% exhibits a high slope adsorption capacity and irreversible sodium loss, which is attributed to the fact that some of the FB molecules were not grafted on the HC surface. The –COOH functional group within FB molecule contributes excess irreversible adsorption capacity. Therefore, the improvement of electrochemical properties is highly correlated with the content of FB molecules.

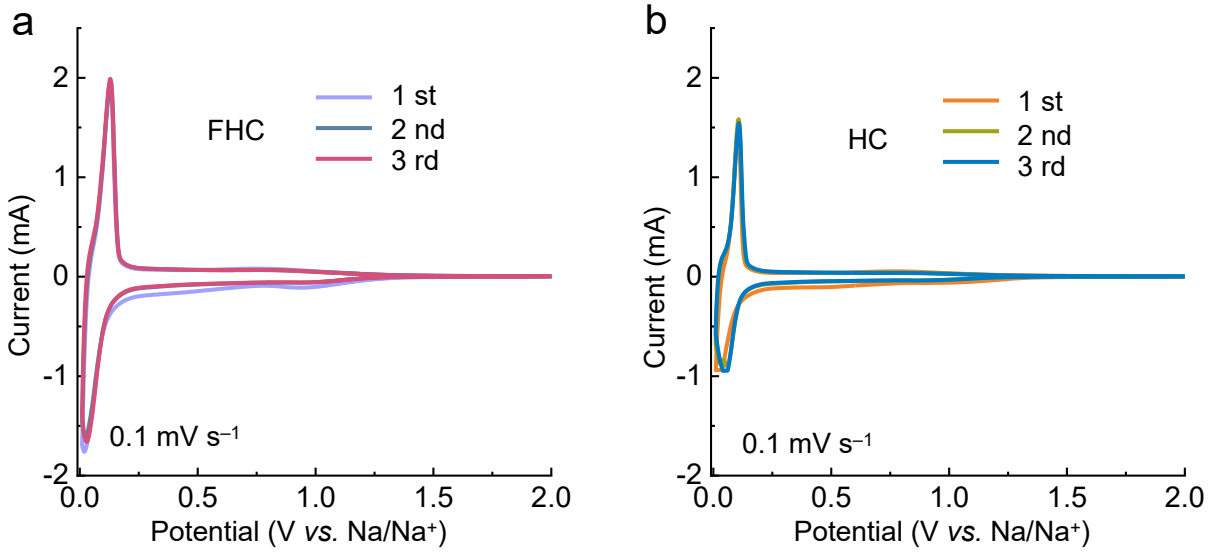

Fig. S12 GCD curves for the first three cycles of (a) FHC and (b) HC.

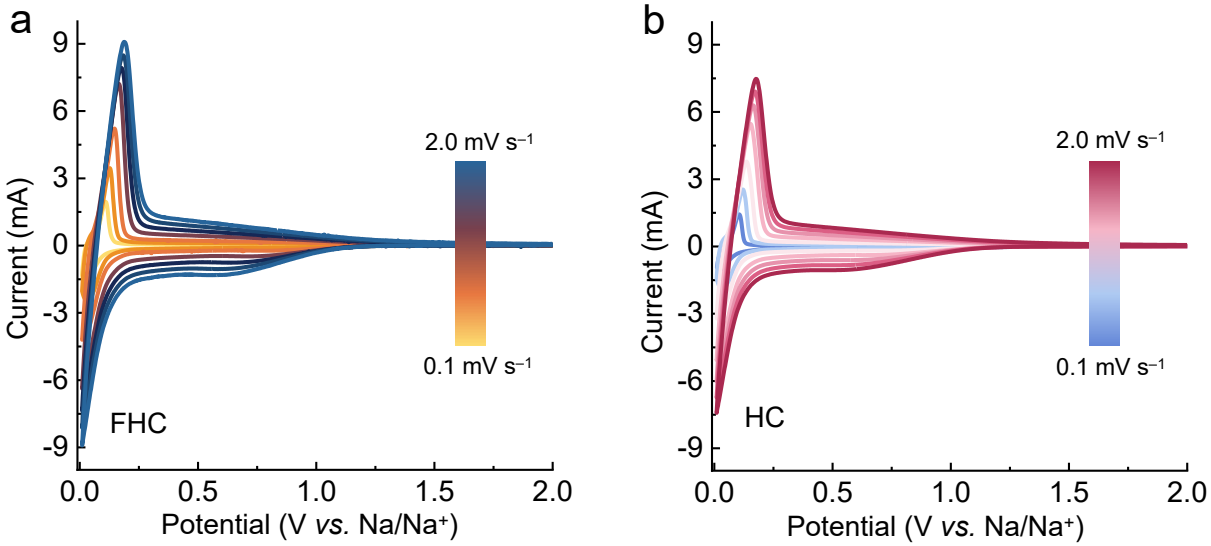

Fig 13 CV profiles of (a) FHC and (b) HC at different scanning rates (from 0.1 mV^{-1}–2.0 mV^{-1}).

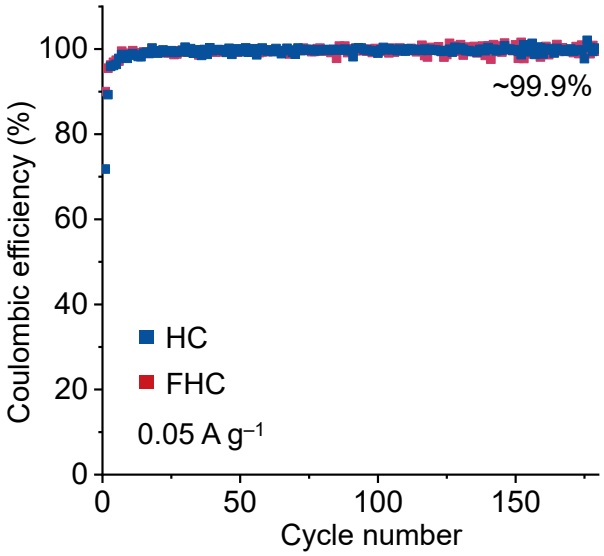

Fig. S14 CE of HC and FHC cycled at 0.05 A g^{-1}.

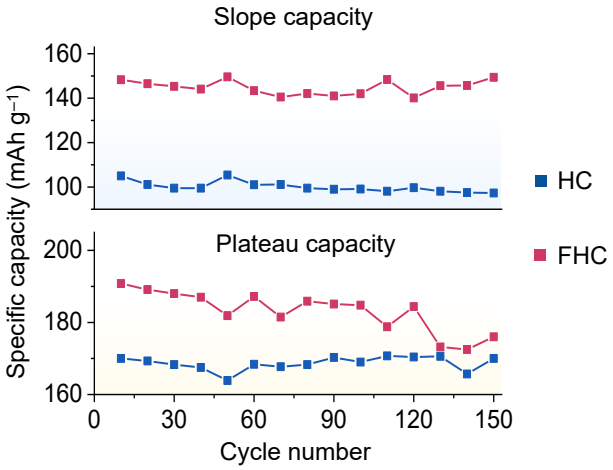

Fig. S15 The capacity contributions of HC and FHC in the slope and plateau region, respectively.

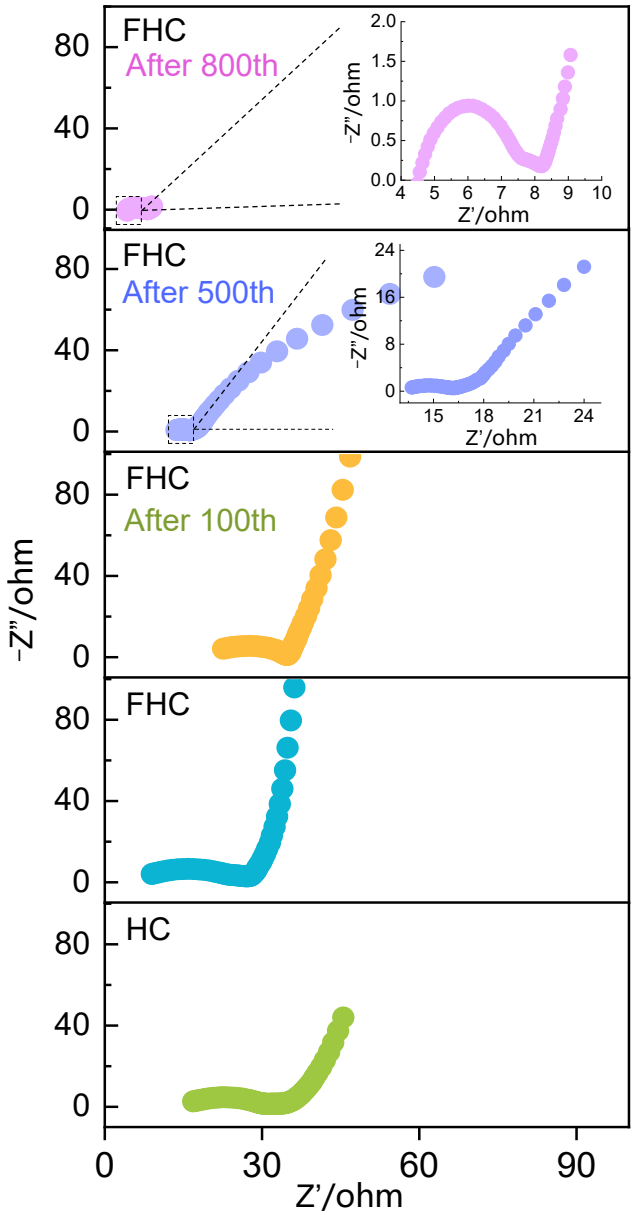

Fig. S16 EIS curves of FHC before and after cycling compared to HC.

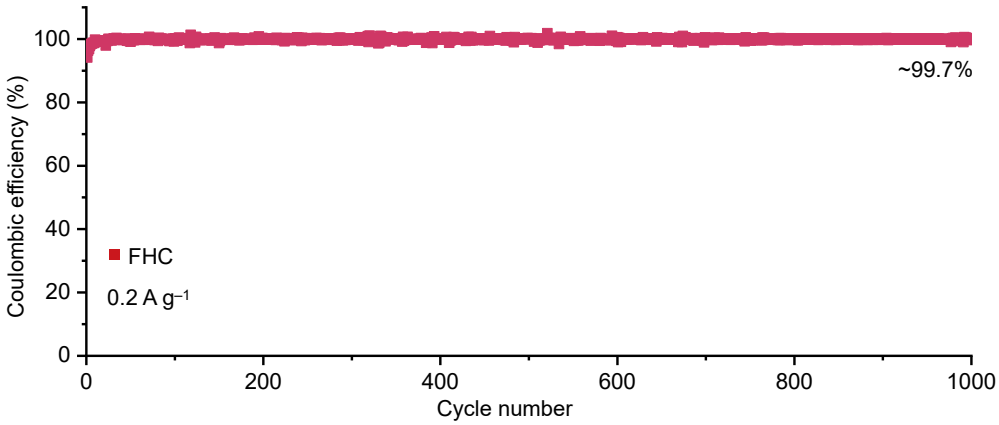

Fig. S17 CE of HC and FHC served at 0.2 A g^{-1}.

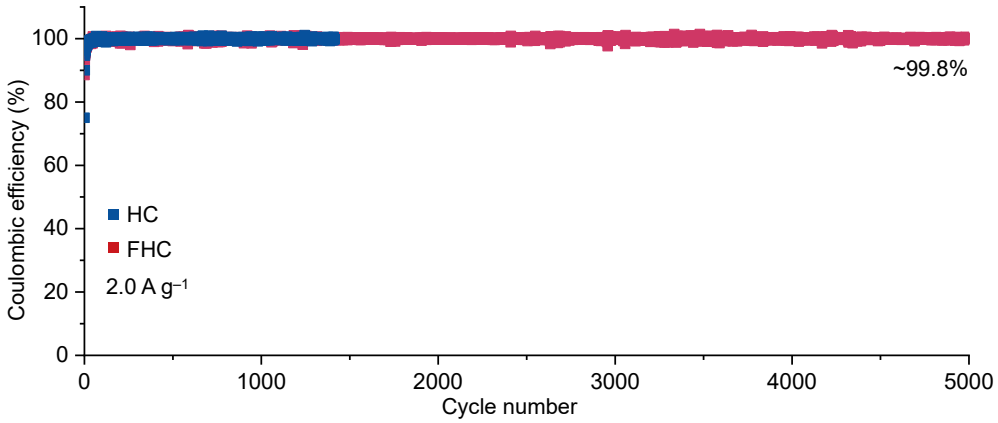

Fig. S18 CE of HC and FHC served at 2.0 A g^{-1}.

To demonstrate the stable formation of SEI, we employed TEM techniques to probe the SEI structure of HC and FHC after cycling at different current densities (0.02 A g^{-1} and 2.0 A g^{-1}), as shown in Fig. S19. At the same current density, a thicker and inhomogeneous SEI was formed on the HC surface than that of the FHC, which can be attributed to the severe decomposition of the electrolyte on the HC surface and the instability of the generated SEI, that in turn, decomposed the electrolyte again on the exposed electrode surface. Especially at high current densities of 2.0 A g^{-1}, a ~30 nm thick SEI was generated on the HC surface after many cycles, contributing to the increased interfacial impedance and the continuously reduced sodium storage capacity (Fig. S19c). Conversely, the SEI formed on the FHC surface showed thin and stable features at different current densities.

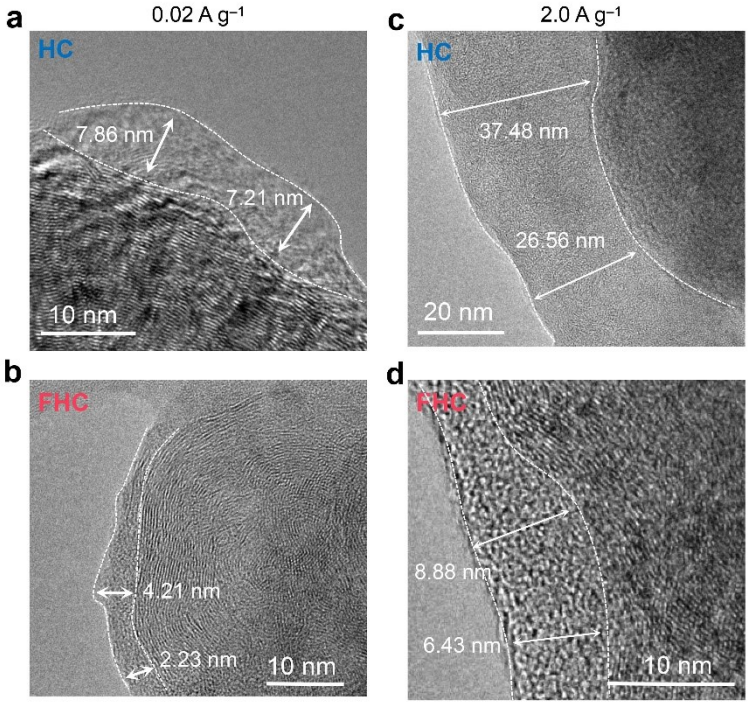

Fig. S19 The SEI structure of HC and FHC after cycling at 0.02 A g^{-1} and 2.0 A g^{-1}.

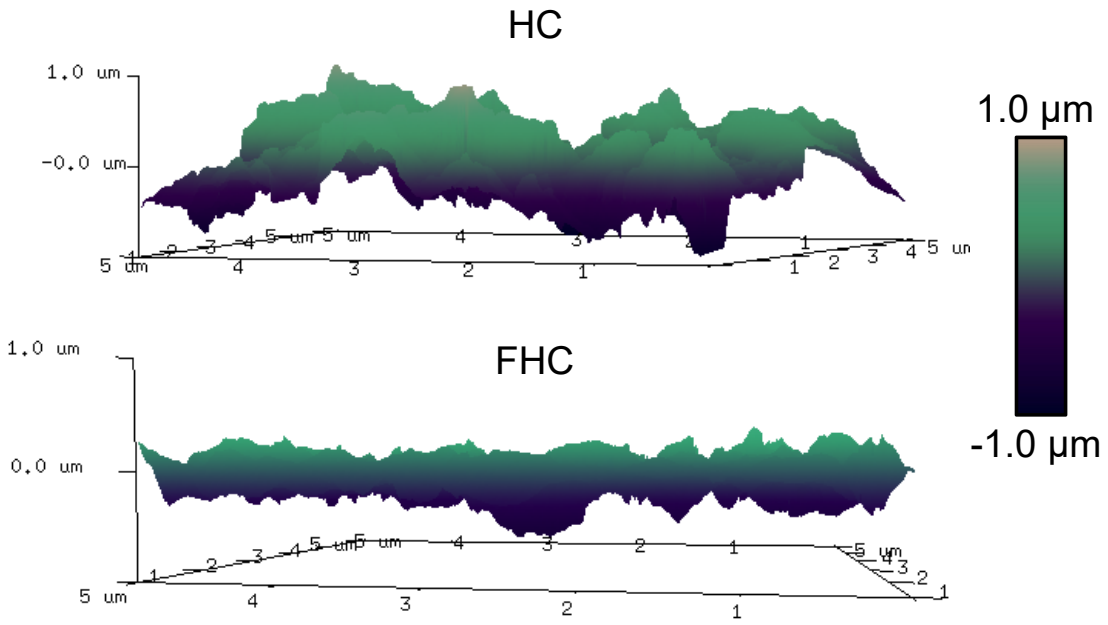

Fig. S20 AFM images of HC and FHC in side-view profile. The SEI formed on the HC surface displayed major height undulations, indicating severe electrolyte decomposition and instability of the formed SEI. Conversely, the optimized the FHC has relatively flat planes, which are induced by the FB molecules to preferentially decompose sodium salts, thereby generating a robust NaF-rich SEI.

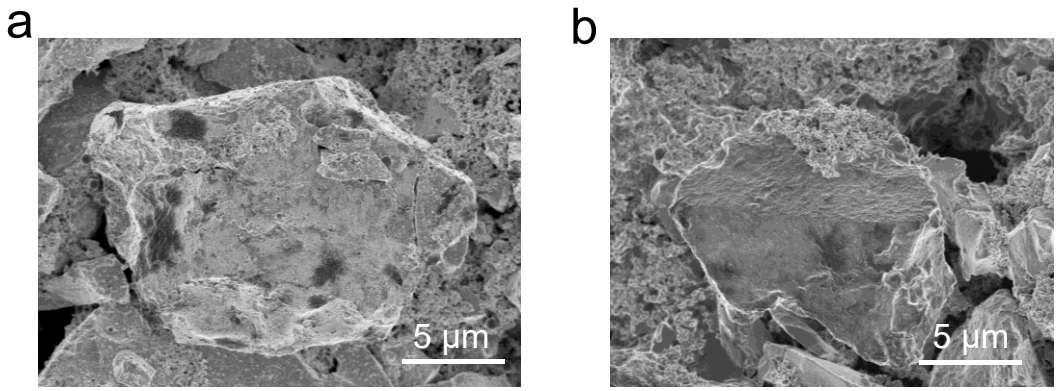

Fig. S21 SEM images of (a) HC and (b) FHC after served 30 cycles.

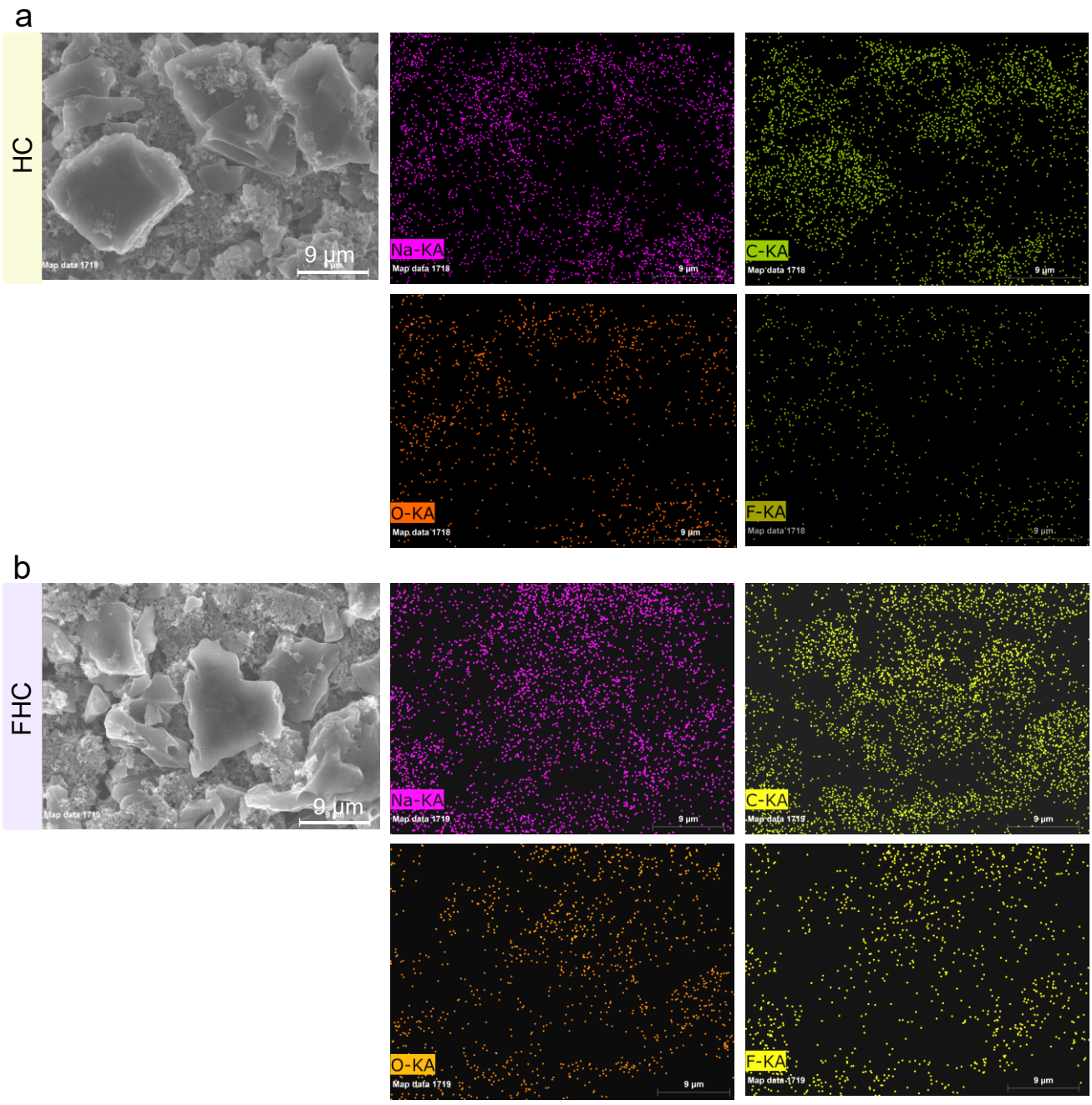

Fig. S22 The elemental distribution of (a) HC and (b) FHC after cycling.

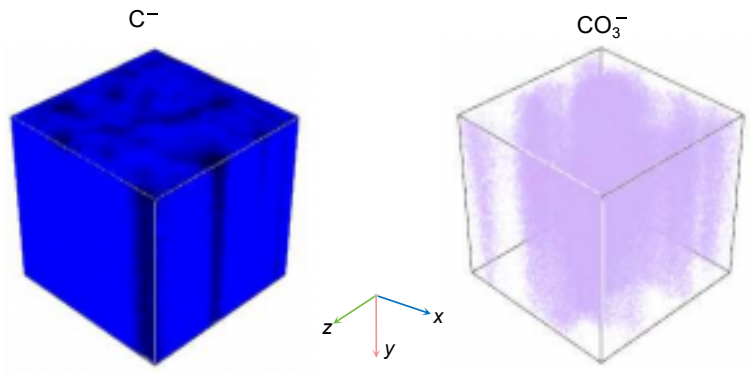

Fig. S23 The distribution of C^- and CO_3^- content in SEI generated on the FHC surface after cycling.

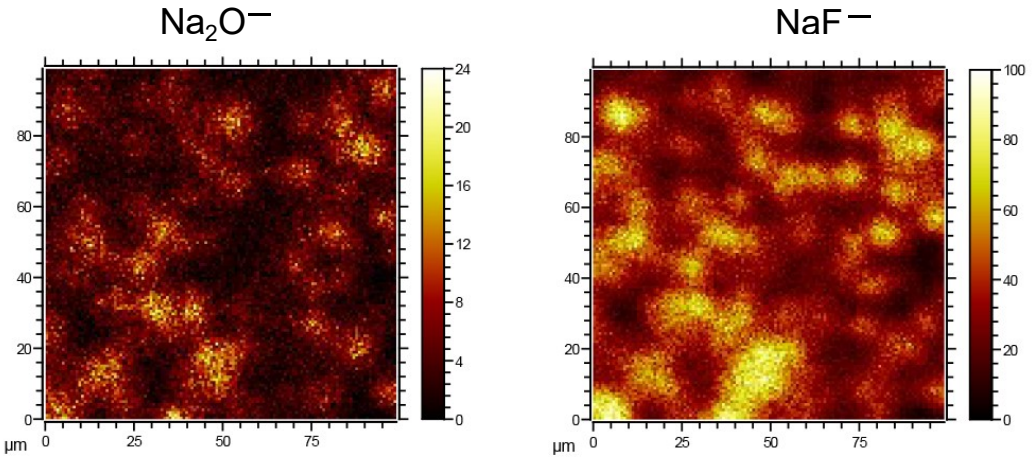

Fig. S24 Two-dimensional image of the Na_2O^- and NaF^- content in the SEI formed on the FHC surface.

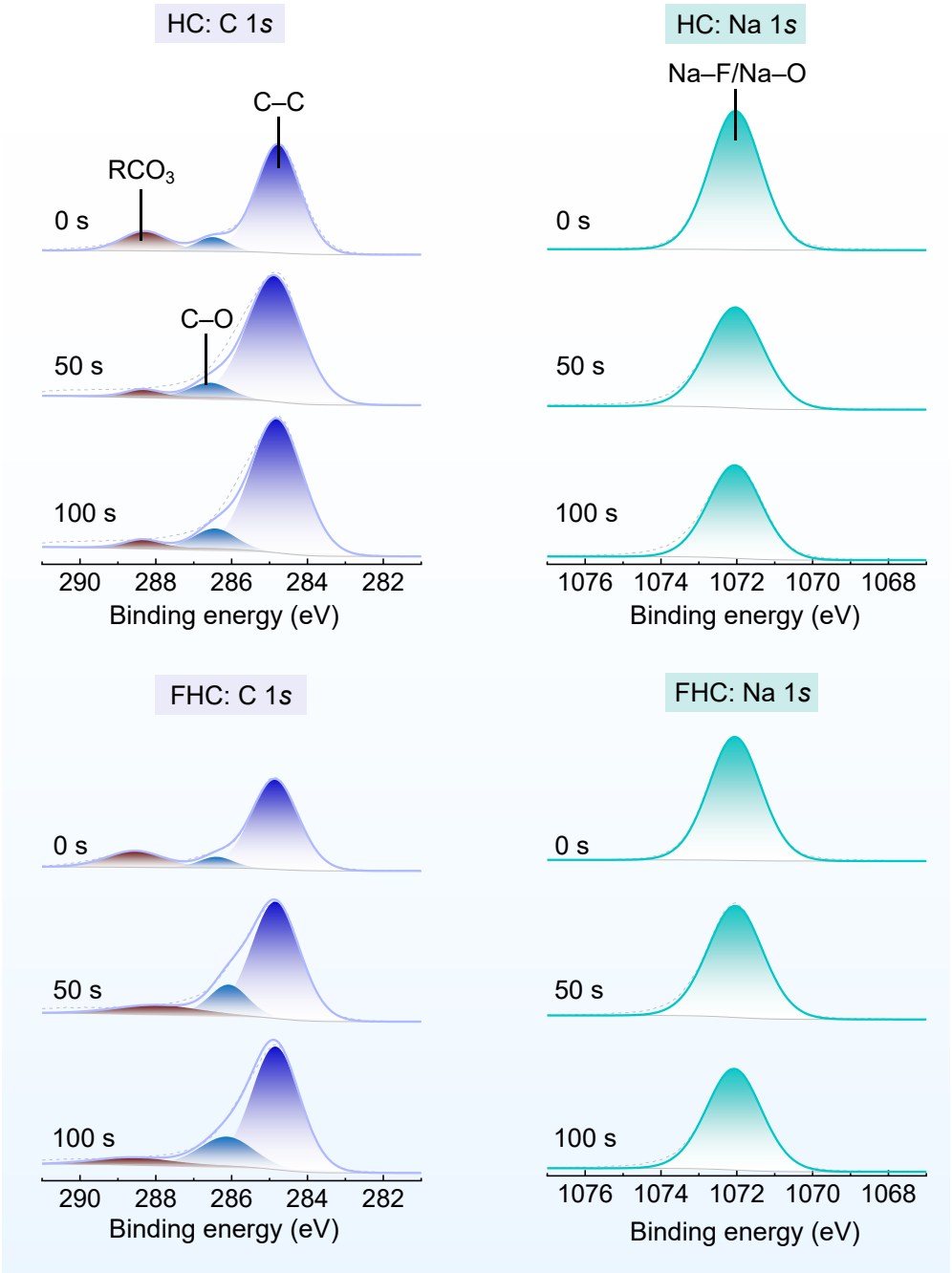

Fig. S25 The XPS C 1*s* and Na 1*s* characteristic peaks of HC and FHC at different etching times.

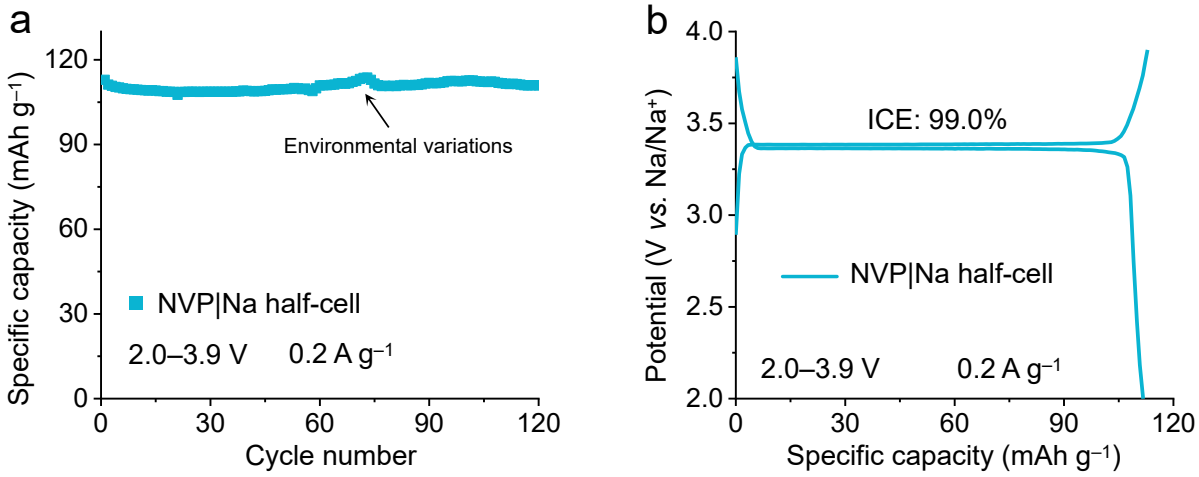

Fig. S26 (a) Cycling performance of the NVP|Na half-cell cycled at 2.0–3.9 V and 0.2 A g^{-1}. (b) ICE profile of the NVP|Na half-cell.

References

1 F. Wang, Z. Jiang, Y. Zhang, Y. Zhang, J. Li, H. Wang, Y. Jiang, G. Xing, H. Liu and Y. Tang, *eScience,* 2024, **4**, 100181.

2 Z. Liu, Z. Lu, S. Guo, Q.-H. Yang and H. Zhou, *ACS Cent. Sci.,* 2023, **9**, 1076–1087.

3 X. Fan, X. Kong, P. Zhang and J. Wang, *Energy Storage Mater.,* 2024, **69**, 103386.

4 M. Liu, F. Wu, Y. Gong, Y. Li, Y. Li, X. Feng, Q. Li, C. Wu and Y. Bai, *Adv. Mater.,* 2023, **35**, 2300002.

5 S. Heng, Z. Cao, Y. Wang, Q. Qu, G. Zhu, M. Shen and H. Zheng, *ACS Appl. Mater. Interfaces,* 2020, **12**, 33408–33420.